Nanotechnology Perceptions
ISSN 1660-6795
www.nano-ntp.com

Chemically Synthesized Aluminum-Functionalized SnO_2 Materials: Structural, Electrical, and Gas Sensing Properties

Swapnil S. Kosalge[1*], Yogita S. Patil[2], Digambar N. Sapkal[3], Pushpinder G. Bhatia[1]

[1]*Department of Physics, Guru Nanak College of Arts, Science and Commerce, Guru Tegh Bahadur Nagar Mumbai-400037, India*

[2]*Department of Physics, COEP technological University, Pune-411045, India.*

[3]*Department of Physics, SICES Degree College, Ambarnath, Mumbai-421591, India.*

Email: kosalgeswapnilres@gmail.com

The co-precipitation method has been used to synthesize aluminum-functionalized SnO_2. The screen-printing method was used to prepare the gas sensing thick films needed to evaluate gas sensing properties. The influence of aluminum functionalization on the structure, electrical conductivity, and gas sensing properties of SnO_2 was examined. XRD analysis revealed that the prepared powder samples were in the cassiterite phase of SnO_2. Furthermore, the crystallite size of SnO_2 was decreased with increased Al percentage. The crystallite size was calculated using the Debye-Scherrer formula. SEM, and EDAX spectroscopy were used for the morphological, and elemental investigations, respectively. LPG, CO, H_2S, and NH_3 gas sensing properties were investigated in the temperature range of 50 ^oC to 300 ^oC. The sensor elements were more selective towards the H_2S gas, and the response time of H_2S was observed in the range of 13–25 S.

Keywords: SnO_2, H_2S gas sensing, Aluminum functionalization.

1. Introduction

Gas sensors play a vital role in safeguarding lives from industrial and household gas leakages. It is also useful in the monitoring of hazards, pollutants, and poisonous gases in the environment. Poisonous gas leakages are hazard near industrial areas [1,2]. few examples of gas leaks in India are: A gas leak was reported in Thane's Ambarnath on 13th September 2024 from the chemical industries during the venting process; On 22nd September 2024, one person died in the incident of the ammonia gas leak from an ice factory at Jalandhar, Punjab. On 30th April 2023, 11 people were died and 9 people were hospitalized during gas leak at Ludhiana, Punjab; On 6th January 2022, because the gas leaked from the tanker 6 people were died and 22 people were hospitalized in an industrial area in Sachin, Surat, Gujrat; from leakage from one chemical company occurred in the industrial area of Badlapur, Maharashtra on June 4th,

2021; residents living 3 km radius from the factory faced breathing issues and eye irritation for a few hours; sulfuric acid was leaked from MIDC Ambernath on October 12th, 2021; 34 people complained about breathing problems; and H_2S gas was leaked from the Indio Amines Limited, Mahad, Maharashtra on January 22nd, 2021.

H_2S gas is used in chemical, pesticide, and pharmaceutical industries to produce sulfuric acid and elemental sulfur, which act as reagents to produce their products. It is used in oil refineries to remove sulphur from petroleum. H_2S gas is frequently found in traces in mines. H_2S is highly toxic and flammable gas. Its effect depends upon the length of time it is inhaled and its concentration in the air. A smaller dose of H_2S breathed in over a period of 3 to 15 minutes may cause watery eyes, chest tightening, and shortness of breath. A large dose of H_2S causes unconsciousness almost instantly, causing brain damage or death. Therefore, it must be monitored and leakage should be detected as soon as possible after it occurs [3–5]. It is essential to install excellent gas sensors not only in industry but also in the vicinity of the industrial areas. As a result, there has been a huge upsurge in the interest of researchers in developing new materials for gas sensors that are cheap, durable, and high performance, and one of the beneficiaries is metal oxide, which has a low cost of production and flexibility associated with its production [6].

To develop new materials, researchers initially investigated pure metal oxide and its functionalization. Recent developments in material characterizations have revealed that materials with low dimensions have improved their characteristic features. Therefore, researchers have been focusing on the functionalization of materials at the nano scale. Functionalization element like Pd [7,8],Pt [9,10], Er [11], Au [12,13], Ce [14,15] etc., improves the gas sensing properties of metal oxide[16].

To prepare functionalized materials at the nanoscale, a variety of methods have been used, like hydrothermal[17,18], sol-gel[19], chemical vapour deposition technique(CVD)[20], and the chemical co-precipitation method [21], Among all these methods, the co-precipitation method is the most cost-effective, simple, and, by changing the synthetic conditions, it is easy to achieve the material with the desired properties [22]

In the present work, we have functionalized the SnO_2 material with Al to get the sensing material. The sensing elements were fabricated using the screen-printing method and their gas sensing properties were studied for LPG, CO, H_2S, and NH_3 gases in the temperature range 50 ºC to 300 ºC

2. Experimental Procedure:

2.1. Synthesis of pure SnO_2 and aluminum-functionalized SnO_2

All the chemicals were AR grade (S D Fine) and used without purification. Five different samples of SnO_2 powder were prepared. The co-precipitation method was used to prepare pure SnO_2 and the aluminum-functionalized SnO_2. Figure 1 shows the flow chart of the synthetic procedure. Only the starting material used was different while preparing aluminum functionalized SnO_2, and the rest of the procedure was same. To prepare Aluminum functionalized SnO_2, $SnCl_4$ $5H_2O$ and Al $(NO_3)_3$ were dissolved in double-distilled water and stirred at room temperature for 30–40 minutes to obtain a homogeneous solution.

Subsequently, liquid ammonia was slowly added into the solution till the pH reached 7, and the solution was kept overnight. In order to remove chloride ions, the sample was continuously washed with ammonium nitrate solution followed by hot water treatment till it showed negative results for the $AgNO_3$ test. Then the precipitate was washed with diluted ethanol to remove the nitrate ions. In the further discussions pure SnO_2 is presented by S_1, SnO_2 with 1wt.% aluminum functionalized SnO_2 is represented as S_2, SnO_2 with 3wt.% aluminum functionalized SnO_2 is represented as S_3, SnO_2 with 5wt.% aluminum functionalized SnO_2 is represented as S_4, and SnO_2 with 7wt.% aluminum functionalized SnO_2 is represented as S5.

2.2. Characterization of the prepared sample:

The structural properties of the prepared samples were characterized using a Rigaku D/MAX – 2500 X-ray diffractometer operating at 40 kV and 15 mA with CuKα radiation (wavelength 1.54056 Å). A field emission scanning electron microscope (FE-SEM, Hitachi S-4800) was used for the microstructural investigation, and energy dispersive X-ray spectroscopy (EDAX) was used to investigate the samples' chemical composition. A transmission electron microscope was used to perform the morphological study (TEM, Tecnai 20). A field emission scanning electron microscope (FE-SEM, Hitachi S-4800) was used for the microstructural investigation, and energy dispersive X-ray spectroscopy (EDAX) was used to investigate the samples' chemical composition. A transmission electron microscope was used to perform the morphological study (TEM, Tecnai 20).

2.3. Preparation of sensor element and performance measurement:

The screen-printing method was used to prepare the sensing element. In the screen-printing method, prepared powder and ethyl cellulose (a temporary binder) were added to an organic binder (mixture of butyl cellulose, butyl carbitol, and terpineol oil) to form a slurry, then the thick films were printed on acetone cleaned glass plates using squeeze and screen printing mesh. The prepared thick films were fired at 500 ^oC for 2 hours to remove organic binder.

For electrical measurements, silver contacts were made by coating silver paste on both sides of the films. The gas sensing properties were studied using a computer-monitored static gas sensing system. The system is made up of a stainless-steel chamber with a gas inlet valve and a sample handling window, a heating arrangement, a sample holder, and a constant voltage source cum picometer Keithley 6487. Sensor responses were studied for H_2S, NH_3, CO_2, and LPG gases in the temperature range of 50 ^oC to 300 ^oC.

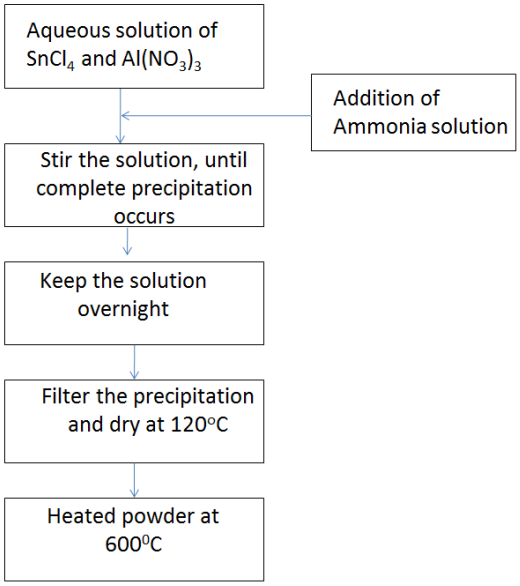

Figure 1: Flow chart of the synthetic procedure

Table 1 Shows number of samples used in the present work

Sr. No.	Sample Name	Wt.% of Aluminum in functionalized SnO_2
1	S_1	0
2	S_2	1
3	S_3	3
4	S_4	5
5	S_5	7

3. Results and discussion:

3.1 Structural characterization:

Figure 2 shows the XRD micrographs of pure and aluminum functionalized SnO_2. All the peaks match the casserite structure of the SnO_2 [23]. (JCPD card no. 88-0287) and have been indexed accordingly. (110), (101), and (200) are the most intense peaks. The substitution of Sn ions by Al ions in these sites results in a slight shift in peak position and inhibition of orientation along (220), (202), and (321) planes, as seen in XRD patterns. Sn^{4+} and Al^{3+} have ionic radii of 0.069nm and 0.053nm, respectively. The difference in their ionic radii produces slight changes in the crystal's microstructure, resulting in a slight shift in the (110) peak to higher angles and the suppression of orientation planes [24]. The average crystallite size was calculated from the (110) peak using the Debuy-Scherrer formula:$d=k\lambda/\beta\cos\theta$, where β is full width half maximum, k is scherrer constant and λ is X-ray wavelength. The crystallite size of S_1, S_2, S_3, S_4, S_5 is found to be 5.43nm 4.04nm, 3.74nm, 3.03 nm, and 2.74nm. Aluminum functionalization causes reduction in particle size by formation of nanostructures.

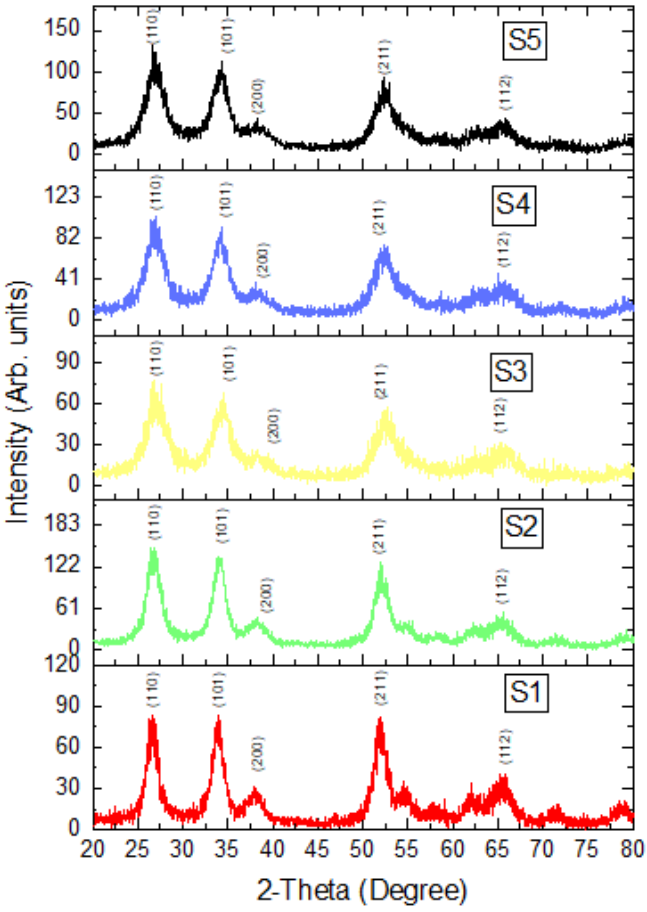

Fig. 2. X-ray diffraction patterns of S_1, S_2, S_3, S_4, and S_5

3.2 Morphological analysis

Aluminum functionalization causes reduction in particle size by formation of nanostructures, was confirmed using FESEM micrographs as shown in figure 3. It seems to be observed that the surface texture of S_4 and S_5 is denser than S_1. S_2, and S_3, as the Al content increases, the amorphous nature of nano particle increases. This result is in good agreement with the XRD patterns. Similar results were observed by N. Kumar et al [24] and Sk. Ahmed [25]. The EDAX patterns of nanoparticles show signals corresponding to Sn, O, and Al elements. The chemical compositions of the samples are shown in table 1, which confirms the formation of the desired sample without impurity. TEM images of pure SnO_2 and Sample S5 is as shown in figure 3, The average crystalline size obtain using XRD analysis and FESEM analysis are in agreement with each other.

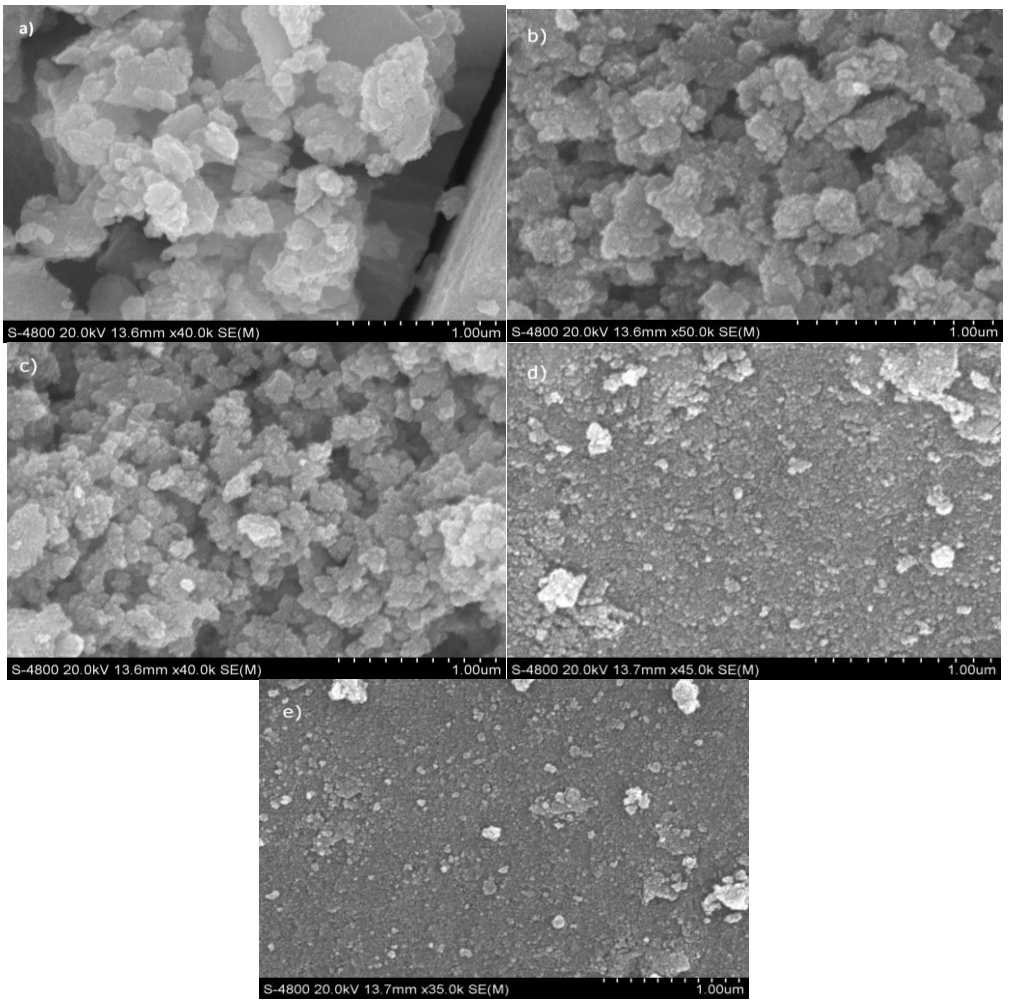

Figure 3: FESEM images of a) S_1, b) S_2, c) S_3, d) S_4, and e) S_5

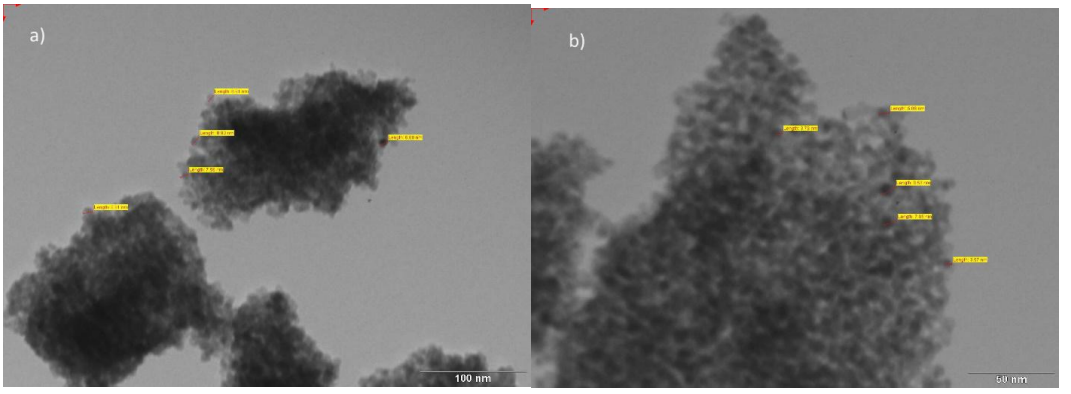

Figure 4. TEM images of a) S_1 and b) S_5

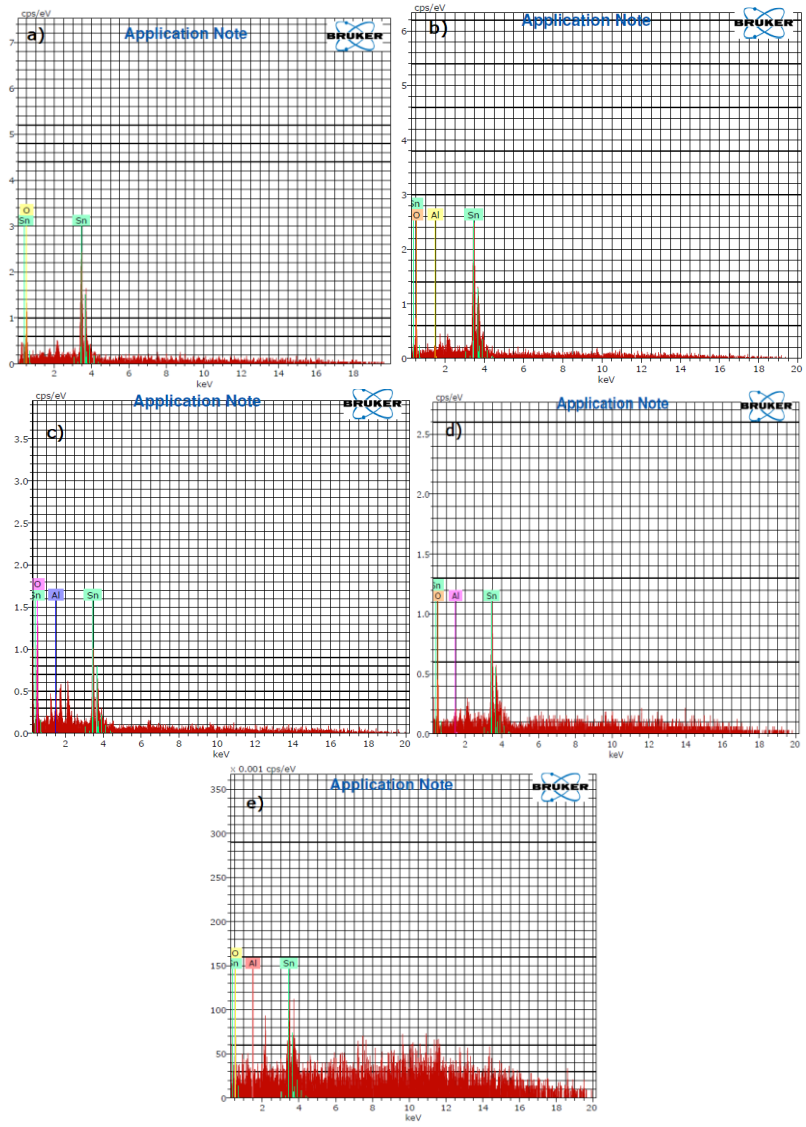

Figure 5: EDAX images of a) S_1, 2) S_2, 3) S_3, 4) S_4, and 5) S_5

Table 2: Elemental analysis of S_1, S_2, S_3, S_4, and S_5

Element (mass %)	Al doping in SnO_2				
	S_1	S_2	S_3	S_4	S_5
Sn	58.97	69.36	36.45	62.33	66.65
O	41.04	30.46	60.95	34.88	25.53
Al	0.00	0.18	2.60	2.79	7.81

3.3 Temperature conductivity dependance

To understand the temperature dependence of conductivity, ln σ was plotted against 1/T of the samples in the range 50 ºC to 300 ºC. Graph showed that the conductivity of Aluminum functionalization SnO_2 decreases as the Al content increases. Decrease in conductivity may be attributed to non-stoichiometric oxygen in the SnO_2 lattice. During the sintering process, Al goes to interstitial sites of the SnO_2 crystal, resulting in an increase in non-stoichiometric oxygen in the SnO_2 lattice, thereby reducing the oxygen vacancy concentration. This leads to an increase in conductivity with an increase in Al content, indeed an earlier investigation confirms that the conductivity of the Al functionalized SnO_2 decreases with increase in Al content [25]. The explanation agrees with the Kröger–Vink defect model reported by Freeman et al[26] .

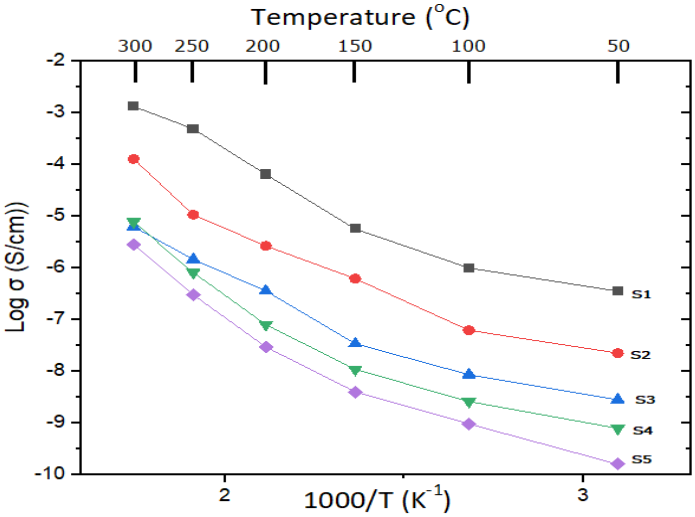

Figure 6: Variation of conductivity in S_1, S_2, S_3, S_4 and S_5 with temperature

3.4 Current –voltage characteristics

The current-voltage characteristics of samples were recorded in the voltage range -8 to 8 volts. The voltage was initially set at -8 volts, then it was decreased to zero and a corresponding current was recorded; a further voltage increase from 0 to 8 volts was recorded. Figure 6 showed a current – voltage of pure SnO_2, and Aluminum functionalization SnO_2 recorded at 50 ºC. As the doping percentage of Al increased, current–voltage characteristics slanted toward the voltage axis, which was attributed to a decrease in conductivity with an increase in doping percentage.

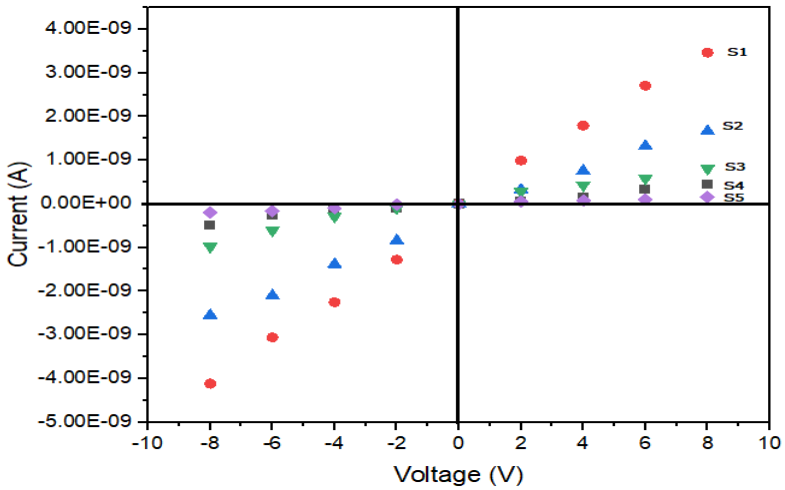

Figure 7: I-V Characteristics of S_1, S_2, S_3, S_4 and S_5

3.5 Gas Sensing Properties:

3.5.1 Effect of operating temperature and H_2S gas concentration

The sensitivity of H_2S gas was calculated using the formula: S = Ra/Rg, where Ra is the settle resistance of the film in air and Rg is the settle resistance of the film in H_2S gas. Initially, the minimum detection limit was found; then the responses of pure and Al functionalized SnO_2 were studied at the different operating temperatures and H_2S gas concentrations.

Figure 7 shows the variation in sensitivity of H_2S gas at different operating temperatures for a 7.5 ppm H_2S gas concentration. The maximum sensitivity was observed at the operating temperature of 200 ^oC for all the samples. The sensitivity of SnO_2 was increased with increasing Al content. The improvement in the sensor response is attributed to the decreasing oxygen vacancy caused by Al doping. A decrease in oxygen leads to an increase in the resistivity of the sample [27]. The same behaviour is reflected in the sensitivity of the sensor.

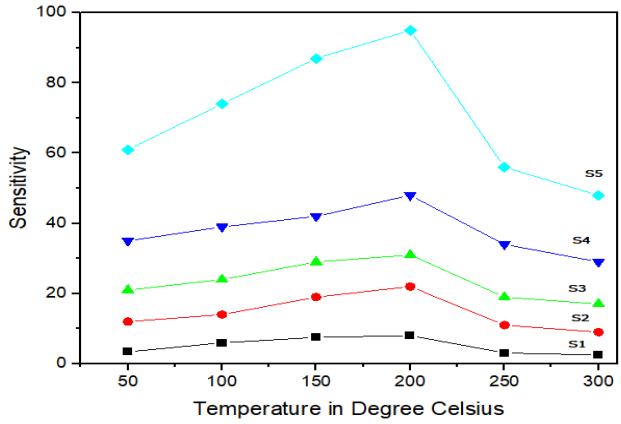

Figure 8: Variation of sensitivity with temperature of S_1, S_2, S_3, S_4 and S_5

Figure 9 depicts film's sensitivity to varied ppm levels for sample S5. As ppm increases, sensitivity also increases. The sensitivity of the film linearly increases from 7.5 ppm to 30 ppm. Thus, the active region of the sensor would be 7.5 ppm to 30 ppm.

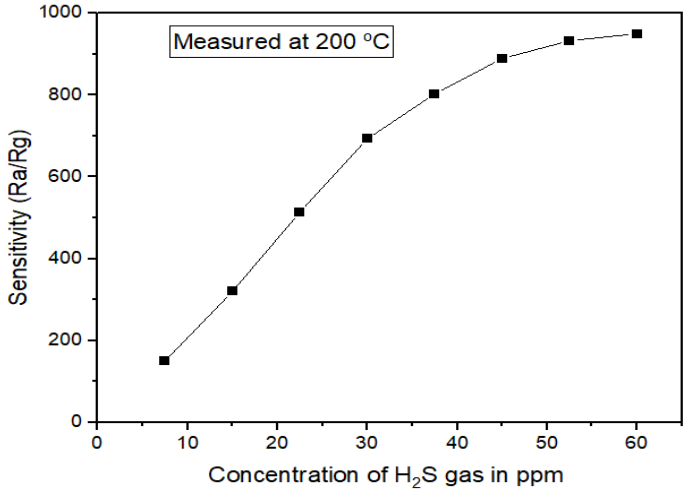

Figure 9: Variation of sensitivity of H_2S gas measured in ppm of sample S_5

3.3.1. Response and recovery time:

The response time was determined for H_2S gas at 200 °C . All the samples sensed the H_2S gas within 13-25 S and recovery was slow at room temperature. The response and recovery time of S_5 are shown in figure 9. The recovery time was decreased by heating the thick film at 500 °C. The recovery time was reduced to few seconds.

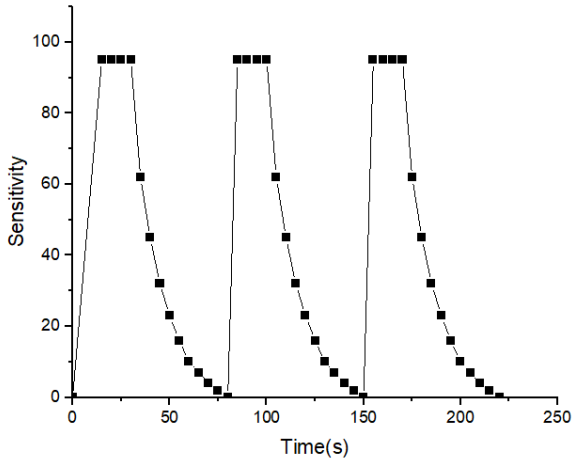

Figure 9: Response and recovery time of S_5

3.3.2. Selectivity for H_2S gas against various gases

Figure 10 shows the selectivity of sample S_5 for H_2S gas at 200 °C. The thick sensor was more selective towards H_2S gas as compared to LPG, CO_2 and NH_3. The selectivity for H_2S is

determined at 7.5 ppm, where as for other gases it was determined at 1000ppm.

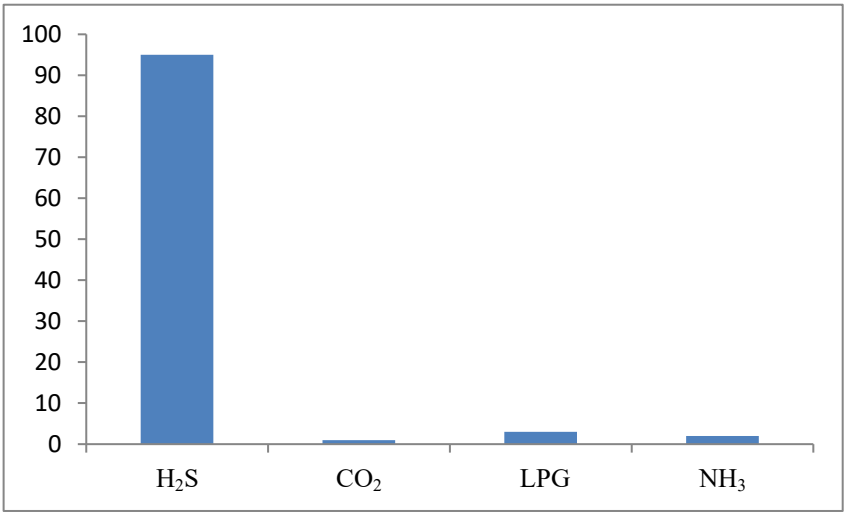

Figure 10: Selectivity of S_5 to H_2S gas

3.4. Gas sensing mechanism:

The mechanism of H_2S gas sensing schematically represented in figure 11. The sensing mechanism of H_2S gas sensing is attributed to the change in resistance of the film by adsorption and, desorption of chemical species O^- and O^{--}. When the SnO_2 is heated in the air at about 150 ºC, chemical species such as O^- and O^{--}gets absorbed over the surface of SnO_2 resulting in formation of depletion layer across the grain as shown in figure (a). When H_2S interacts with the SnO_2 following reaction occurs

$$H_2S_{(gas)} + 3O^-_{(ads)} \longrightarrow H_2O_{(gas)} + SO_{2(gas)} + 3e^-$$

During this process width of the depletion region decreases and resistance of the film decreases as shown in figure (b)

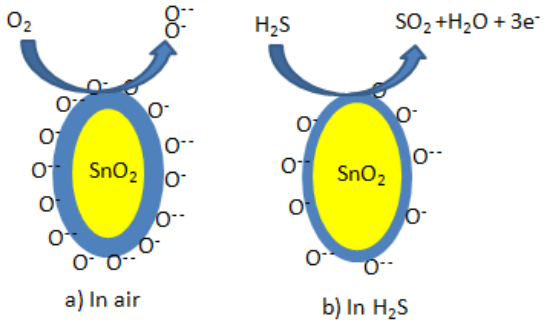

Figure 11: H_2S gas sensing mechanism

4. Conclusion:

Based on observations and experimental evidence, the following conclusions can be drawn.

1) Nano crystalline SnO_2 and aluminum functionalized SnO_2 samples were successfully synthesized using co-precipitation method. The crystalline size of synthesized materials is of the order of 3-6 nm.

2) SnO_2 and aluminium functionalized SnO_2 thick films were successfully manufactured using the screen-printing method; the conductivity of the aluminium functionalized SnO_2 thick films is lower than that of the pure SnO_2 thick film, and the I-V characteristics of the entire films are ohmic in nature.

3) The sensor element based on 7wt.% aluminium functionalized SnO_2 thick film exhibited good response to 7.5 ppm H_2S gas at 200 ^{o}c.

4) The sensor element based on 7wt.% aluminium functionalized SnO_2 thick film is more selective toward the H_2S gas as compared to CO_2, LPG and NH_3. Also it exhibits quick response (13-15S) and good recovery.

References

[1] Y. He, M. Jiao, A Mini-Review on Metal Oxide Semiconductor Gas Sensors for Carbon Monoxide Detection at Room Temperature, Chemosensors 12 (2024). https://doi.org/10.3390/hemosensors12040055.

[2] Y. Wu, M. Lei, X. Xia, Research Progress of MEMS Gas Sensors: A Comprehensive Review of Sensing Materials, Sensors 24 (2024) 8125. https://doi.org/10.3390/s24248125.

[3] A. Bibi, K.S. Santiago, J.-M. Yeh, H_2S gas sensor based on biodegradable-electroactive polyurethane-urea and activated carbon composite derived from coconut shell waste, n.d. https://ssrn.com/abstract=4181245.

[4] T.S. Carpenter, S.M. Rosolina, Z.L. Xue, Quantitative, colorimetric paper probe for hydrogen sulfide gas, Sens Actuators B Chem 253 (2017) 846–851. https://doi.org/10.1016/J.SNB.2017.06.114.

[5] Y. Lu, D. Wang, W. Lv, Y. Xia, K. Ou, Y. Li, Z. Du, Y. He, J. Dai, S. Wu, J. Luo, Y. Tang, Surface acoustic wave hydrogen sulfide gas sensors based on porous SnO_2-SiO_2 composite films, Sens Actuators B Chem 417 (2024) 136117. https://doi.org/10.1016/J.SNB.2024.136117.

[6] C. Wang, L. Yin, L. Zhang, D. Xiang, R. Gao, Metal oxide gas sensors: Sensitivity and influencing factors, Sensors 10 (2010) 2088–2106. https://doi.org/10.3390/s100302088.

[7] Z. Cai, S. Park, Synthesis of Pd nanoparticle-decorated SnO_2 nanowires and determination of the optimum quantity of Pd nanoparticles for highly sensitive and selective hydrogen gas sensor, Sens Actuators B Chem 322 (2020). https://doi.org/10.1016/j.snb.2020.128651.

[8] D.H. Baek, J. Kim, MoS_2 gas sensor functionalized by Pd for the detection of hydrogen, Sens Actuators B Chem 250 (2017) 686–691. https://doi.org/10.1016/j.snb.2017.05.028.

[9] Y.P. Sun, Y.F. Zhao, H. Sun, F.C. Jia, P. Kumar, B. Liu, Synthesis and room-temperature H_2S sensing of Pt nanoparticle-functionalized SnO_2 mesoporous nanoflowers, J Alloys Compd 842 (2020). https://doi.org/10.1016/j.jallcom.2020.155813.

[10] T. Ai, J. Zhang, J. Li, Y. Zhang, Y. Yin, J. Lu, Ultrafast response of Pt functionalized $Fe_2(MoO_4)_3$ nanoflower gas sensors for ultra-low ppm level H_2 gas detection, J Alloys Compd 970 (2024) 172567. https://doi.org/10.1016/J.JALLCOM.2023.172567.

[11] M.K. Sohal, A. Mahajan, S. Gasso, S. V. Nahirniak, T.A. Dontsova, R.C. Singh, Modification of SnO2 surface oxygen vacancies through Er doping for ultralow NO_2 detection, Mater Res Bull 133 (2021). https://doi.org/10.1016/j.materresbull.2020.111051.

[12] X. Wang, F. Liu, X. Chen, G. Lu, X. Song, J. Tian, H. Cui, G. Zhang, K. Gao, SnO_2 core-shell hollow microspheres co-modification with Au and NiO nanoparticles for acetone gas sensing, Powder Technol 364 (2020) 159–166. https://doi.org/10.1016/j.powtec.2020.02.006.

[13] L. Wang, S. Wang, M. Xu, X. Hu, H. Zhang, Y. Wang, W. Huang, A Au-functionalized ZnO nanowire gas sensor for detection of benzene and toluene, Physical Chemistry Chemical Physics 15 (2013) 17179–17186. https://doi.org/10.1039/c3cp52392f.

[14] G. Fedorenko, L. Oleksenko, N. Maksymovych, I. Vasylenko, Cerium-doped SnO2 nanomaterials with enhanced gas-sensitive properties for adsorption semiconductor sensors intended to detect low H_2 concentrations, J Mater Sci 55 (2020) 16612–16624. https://doi.org/10.1007/s10853-020-05199-w.

[15] N. Sharma, S.P. Choudhury, Gas sensing using metal oxide semiconductor doped with rare earth elements: A review, Materials Science and Engineering: B 307 (2024) 117505. https://doi.org/10.1016/J.MSEB.2024.117505.

[16] A.G. Schiopu, D.M. Iordache, M. Oproescu, L.M. Cursaru, A.M. Ioța, Tailoring the Synthesis Method of Metal Oxide Nanoparticles for Desired Properties, Crystals (Basel) 14 (2024). https://doi.org/10.3390/cryst14100899.

[17] J.A. Darr, J. Zhang, N.M. Makwana, X. Weng, Continuous Hydrothermal Synthesis of Inorganic Nanoparticles: Applications and Future Directions, Chem Rev 117 (2017) 11125–11238. https://doi.org/10.1021/acs.chemrev.6b00417.

[18] L. Wang, Z. Lou, T. Zhang, H. Fan, X. Xu, Facile synthesis of hierarchical SnO_2 semiconductor microspheres for gas sensor application, Sens Actuators B Chem 155 (2011) 285–289. https://doi.org/10.1016/j.snb.2010.12.036.

[19] D. Bokov, A. Turki Jalil, S. Chupradit, W. Suksatan, M. Javed Ansari, I.H. Shewael, G.H. Valiev, E. Kianfar, Nanomaterial by Sol-Gel Method: Synthesis and Application, Advances in Materials Science and Engineering 2021 (2021). https://doi.org/10.1155/2021/5102014.

[20] F. Shao, M.W.G. Hoffmann, J.D. Prades, R. Zamani, J. Arbiol, J.R. Morante, E. Varechkina, M. Rumyantseva, A. Gaskov, I. Giebelhaus, T. Fischer, S. Mathur, F. Hernández-Ramírez, Heterostructured p-CuO (nanoparticle)/n-SnO2 (nanowire) devices for selective H_2S detection, Sens Actuators B Chem 181 (2013) 130–135. https://doi.org/10.1016/j.snb.2013.01.067.

[21] Y. Patil, R.B. Pedhekar, S. Patil, S. Kosalge, F.C. Raghuvanshi, Chemically synthesized ZnO and Cd-ZnO thick films as Ethanol sensor, IOP Conf Ser Mater Sci Eng 1126 (2021) 012046. https://doi.org/10.1088/1757-899x/1126/1/012046.

[22] H. Wang, X. Xu, J. Zhang, C. Li, A Cost-Effective Co-precipitation Method for Synthesizing Indium Tin Oxide Nanoparticles without Chlorine Contamination, J Mater Sci Technol 26 (2010) 1037–1040. https://doi.org/10.1016/S1005-0302(10)60171-5.

[23] A. Sivashanmugam, T.P. Kumar, N.G. Renganathan, S. Gopukumar, M. Wohlfahrt-Mehrens, J. Garche, Electrochemical behavior of Sn/SnO_2 mixtures for use as anode in lithium rechargeable batteries, J Power Sources 144 (2005) 197–203. https://doi.org/10.1016/j.jpowsour.2004.12.047.

[24] N. Kumari, A. Ghosh, S. Tewari, A. Bhattacharjee, Synthesis, structural and optical properties of Al doped SnO_2 nanoparticles, Indian Journal of Physics 88 (2014) 65–70. https://doi.org/10.1007/s12648-013-0387-0.

[25] S.F. Ahmed, S. Khan, P.K. Ghosh, M.K. Mitra, K.K. Chattopadhyay, Effect of Al doping on the conductivity type inversion and electro-optical properties of SnO_2 thin films synthesized by sol-gel technique, J Solgel Sci Technol 39 (2006) 241–247. https://doi.org/10.1007/s10971-006-7808-x.

[26] 26 Freeman, (n.d.).

[27] S.K. Sinha, S.K. Ray, I. Manna, Effect of Al doping on structural, optical and electrical properties of SnO_2 thin films synthesized by pulsed laser deposition, Philosophical Magazine 94 (2014) 3507–3521. https://doi.org/10.1080/14786435.2014.962641.